CHAPTER I

INTRODUCTION

A. Eruption and Impact of the Mount Pinatubo Volcano

The Mount Pinatubo volcano on the island of Luzon (15°N, 120°E), Philippines, erupted catastrophically in June 1991 after more than 600 years of inactivity. The most powerful among a series of eruptions happened on 15 June 1991. The volume of the eruption was about 5 km^3 of magma. Almost 150 m of the mountain was blasted away by this eruption. The volcanic plume, which consisted of volcanic ash and gaseous sulfur dioxide (SO_2), reached as high as 30 km. Heavy seasonal rainfall washed away these volcanic ash flows and caused massive floods and destruction of property and land. More than 200,000 people were forced to evacuate and more than 300 people died, largely owing to the collapse of roofs (Newhall and Punongbayan 1996).

A few selected major volcanic eruptions in the past two centuries are listed in Table 1.1. The largest eruption was Tambora in 1815. The second largest was Krakatau in 1883. Mount Pinatubo is the third largest. The Pinatubo eruption injected about $20x10^{12}$ g (20 Tg) of gaseous SO_2 into the stratosphere, which is about three times as much as El Chichón. This gas reached the stratosphere and circled the globe in three weeks (Blutch *et al.* 1992). The maximum mass loading of stratospheric sulfate aerosol, which was converted from SO_2, estimated by the Stratospheric Aerosol and Gas Experiment–II (SAGE–II) satellite was about 30 Tg in the last few months of 1991 (McCormick *et al.* 1995). The background sulfate–aerosol mass loading in the stratosphere is usually less than 1.0 Tg. The Pinatubo aerosol particles were transported to high latitudes and spread over the world. They were suspended in the atmosphere for several years and caused the largest aerosol perturbation to the stratosphere in this century.

Table 1.1. *Major volcanic eruptions in the past two centuries. VEI (Volcano Explosivity Index) is a scale determined by a number of factors that can be observed during an eruption (Newhall and Self 1982). These data were collected from McCormick et al. (1995), Rampino and Self (1984), Robock and Mao (1995) and the Volcano World (http://volcano.und.nodak.edu/). Not all data are available.*

Eruption	Date	Lat /Lon	VEI	Magma Volume (km^3)	Column Height (km)	SO_2 (Tg)	Sulfate Aerosols (Tg)
Tambora	Apr 1815	8°S, 118°E	7	> 50	> 40		200
Krakatau	Aug 1883	6°S, 105°E	6	> 10	> 40		50
Santa Maria	Oct 1902	15°N, 92°E	6	~ 9	> 30		< 20
Katmai	Jun 1912	58°N, 155°W	6	15	> 27		< 20
Agung	Mar 1963	8°S, 116°E	4	0.3 – 0.6	18	12	10 – 20
St. Helens	May 1980	46°N, 122°E	5	0.35	22	2	0.3
El Chichón	Apr 1982	17°N, 93°E	5	0.3 – 0.35	26	7	10 – 20
Mt. Pinatubo	Jun 1991	15°N, 120°E	6	5	30	20	30

The impact of a volcanic eruption on the earth–atmosphere system is multi–fold. Fig. 1.1 illustrates the dominant processes involving the formation and deposition of volcanic aerosols and the most important chemical, radiative and dynamical effects of these aerosols on the atmosphere. During a volcanic eruption, a large amount of SO_2 injected into the stratosphere is converted into

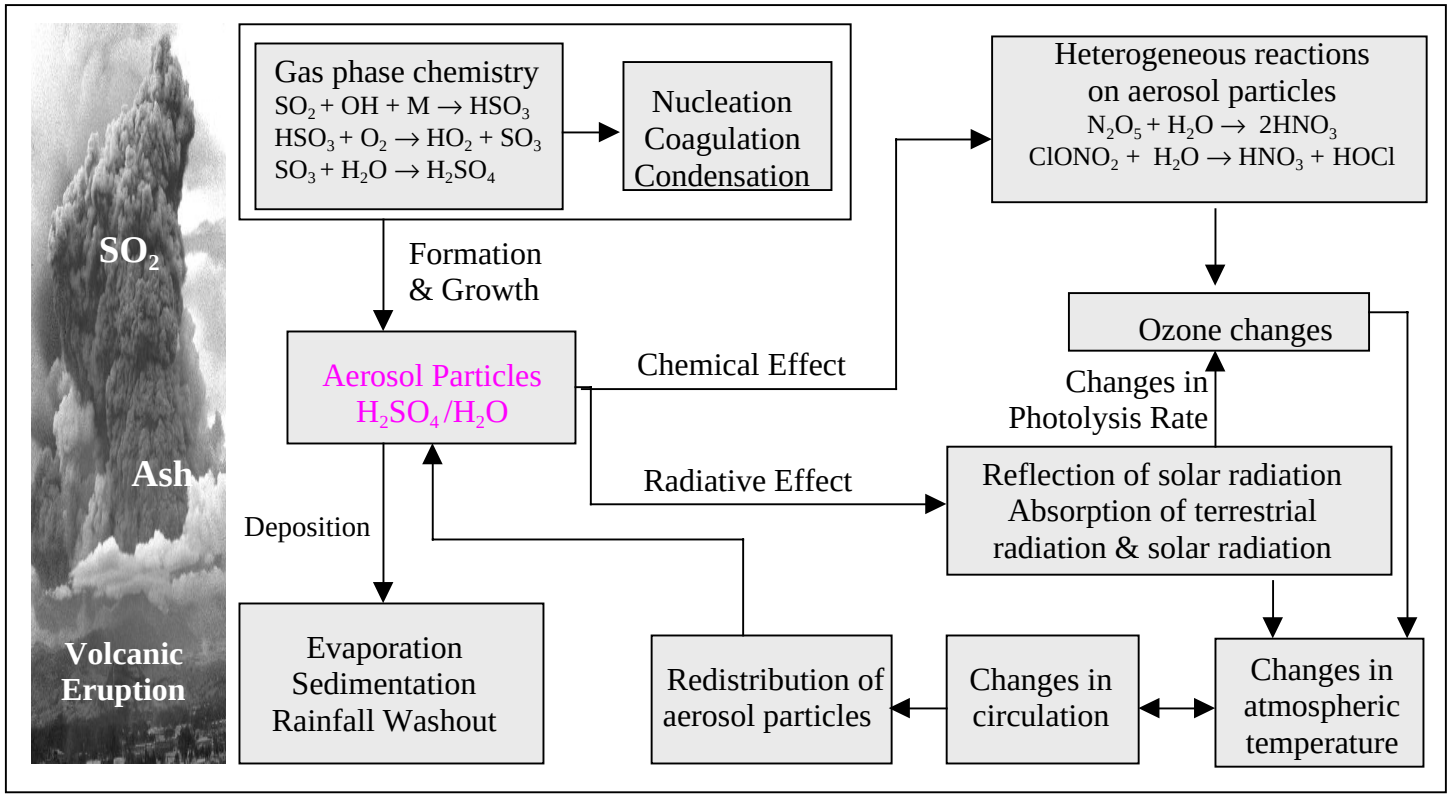

Fig. 1.1. *A schematic diagram illustrating the formation and deposition of the stratospheric aerosol particles after a volcanic eruption and their influences on the atmospheric chemical reactions, radiation budget, temperature and circulation.*

H_2SO_4 vapor by OH oxidation. Saturated H_2SO_4 vapor condenses to form aerosol particles (H_2SO_4/H_2O solution). These aerosol particles interact with other aerosol particles in the stratosphere and grow through further condensation, homogeneous and heterogeneous nucleation, and coagulation. They also evaporate when the H_2SO_4 vapor becomes unsaturated. Depending on their size and atmospheric conditions these aerosol particles can stay in the stratosphere for a few days up to several years before they fall into the troposphere under gravitational force. In the troposphere the aerosol particles are often washed out quickly by precipitation, and eventually come down to the earth's surface. Volcanic aerosol particles in the stratosphere can cause large perturbations to the atmospheric chemical constituents and radiation budget. For instance, the enhanced heterogeneous reactions on the surface of the aerosol particles can convert more reactive nitrogen into inactive nitric acid and lead to an enhancement in the concentration of reactive chlorine. The two heterogeneous reactions in Fig. 1.1 involving N_2O_5 and $ClONO_2$ play a key role in producing the increased reactive chlorine and thus leading to the increased ozone destruction often observed in the stratosphere after volcanic eruptions (McCormick *et al.* 1995). Volcanic aerosol particles can disturb the atmospheric radiation budget by reflecting solar radiation, primarily in the ultra–violet (UV) and visible bands, back into space and by absorbing terrestrial radiation and part of the solar radiation in the near–infrared region. The disturbance of the radiation budget causes atmospheric temperature and, in turn, atmospheric circulation to change. The reflection of solar radiation by aerosol particles also increases the photodissociation rates of certain chemical reactions in the stratosphere above the aerosol cloud because of the increased solar UV radiation, and thus leads to decrease in the concentrations of several chemical compounds such as ozone (Tie *et al.* 1994). Furthermore, the change in the atmospheric circulation modifies the transport and, consequently, the distribution of volcanic aerosol particles

over the globe. All these processes are linked to each other and create a complex picture of how volcanic eruptions affect the earth–atmospheric system.

B. Review and Perspective

The Pinatubo eruption is not exceptional from other major historical volcanic eruptions in the sense of its disastrous impact on human beings and effect on the earth–atmosphere system, but it has been the best–observed volcanic eruption on record. Satellite, balloon, lidar, aircraft and ground–based measurements provided rich information about the formation and evolution of the aerosol cloud and the radiative and chemical effects of the aerosol particles on the atmosphere during and after the Pinatubo eruption (Russell *et al.* 1996, and references therein). These measurements provided us a rare opportunity to understand better the natural variability of the climate system and human–induced climate changes, and to test the various dynamical, radiative and chemical models that have been used to study past and present climate and to predict possible future climate changes.

Some numerical simulations have been performed to understand the formation, growth and deposition of the Pinatubo aerosol particles and the chemical effect of these aerosol particles on atmospheric constituents. For example, Zhao *et al.* (1995) used a 1–D model to study the gas–phase sulfur photochemistry, gas–to–particle conversion of sulfur dioxide and aerosol microphysical processes (condensational growth, nucleation, coagulation and gravitational sedimentation). Pudykiewicz and Dastoor (1995) simulated the distribution of the Pinatubo aerosol with a simplified three–dimensional dynamical model. Kinnison *et al.* (1994) used a 2–D chemical–radiative–transport model to investigate the effect of the Pinatubo aerosol particles on atmospheric chemistry, especially ozone depletion. Xie *et al.* (1994) used a 2–D chemical–radiative–transport model with aerosol microphysics to simulate the formation of the

Pinatubo aerosol particles and their influences on atmospheric chemical components, including ozone. Recently, Knight *et al.* (1998) simulated the Antarctic ozone hole in two southern–hemisphere spring seasons following the Pinatubo eruption using a 3–D stratospheric model with simplified dynamics, but with rather detailed radiative transfer and photochemistry. The present study is focused on the radiative forcing of the Pinatubo eruption, and the influences of the forcing on surface–air temperature and atmospheric temperature and circulation.

1. Optical Properties and Radiative Forcing

In addition to its indispensable role in simulating the climatic impact of the Pinatubo eruption by atmospheric general circulation models (GCM), an accurate estimate of the radiative forcing of the Pinatubo aerosol is also essential to obtain a better understanding of the observed decadal–scale climate changes. It has been hypothesized (Pollack *et al.* 1976) that the observed increase in global–mean surface–air temperature from the 1850's to the present is in part due to the decrease in the number of major volcanic eruptions from the 19th to the 20th century. This decrease results in a relative warming of the climate. The 1995 IPCC report (Schimel *et al.* 1996) estimated that the decadal–mean radiative forcing of volcanic aerosols might have varied by as much as 1.5 W/m^2 since 1850. However, it has been difficult to test this hypothesis quantitatively because the estimate of the radiation forcing of historical volcanic eruptions has large uncertainty owing to the lack of adequate observations. For the Pinatubo eruption the estimate of aerosol radiative forcing by a few theoretical models (Chou *et al.* 1984; Lacis *et al.* 1992; Minnis *et al.* 1993; Stowe *et al.* 1992) varies by a factor of two to three (Andronova *et al.* 1999). The Pinatubo aerosol radiative forcing can be better estimated by using comprehensive radiative–transfer models (RTM) since the Pinatubo eruption has been better characterized by modern observations. An accurate estimate of the Pinatubo radiative forcing will also help us understand other historical volcanic eruptions better.

The most recent calculation of the Pinatubo aerosol radiative forcing was carried out by Stenchikov *et al.* (1998) using the ECHAM4 19–layer atmospheric GCM with prescribed aerosol optical properties (extinction efficiency, single–scattering albedo and asymmetry). However, the ECHAM4 GCM has a relatively coarse spectral–radiative resolution and a coarse vertical resolution in the upper stratosphere. It has only two spectral bands in the solar and 7 spectral bands in the longwave. The top layer of the model extends from 0 hPa to 20 hPa. The plume of the Pinatubo aerosol extended higher than 20 hPa. In the present study, the UIUC 24–layer stratosphere–troposphere GCM will be used to recalculate the Pinatubo aerosol radiative forcing. This model has 9 spectral bands in the solar and 11 spectral bands in the longwave. It has 10 layers between 100 hPa and 1 hPa, with constant log–pressure thickness.

It should be indicated that even though the Pinatubo eruption has been the best observed in history, the observational database on its own is still not adequate enough for GCMs to perform global studies. Ground–based observations had limited coverage in space and time. Satellite observations had limited spectral and/or spatial resolutions and some measurement mistakes (Russell *et al.* 1996). For example, SAGE–II measures aerosol extinction at four wavelengths (0.38, 0.45, 0.525, and 1.02 μm) with an approximate 1 km fine vertical resolution. However, its temporal and horizontal resolutions are coarse. No SAGE–II data were available at the time and latitude of the greatest optical depth following the Pinatubo eruption (August–September 1991; 5°N ~ 20°S) because at wavelength 0.525 μm optical depths of about 0.2 or more saturated the instrument. On the other hand, AVHRR, a broad–band scanner, has rather fine horizontal (~1.1 km) and temporal (~ one week) resolutions, and is able to detect aerosol optical depth up to about 2, at which value the aerosol signal cannot be separated from water clouds. However, it has no inherent vertical resolution. Stratospheric aerosols with optical depths less than 0.01 can not be detected and separated from the tropospheric aerosols. The standard product is available at only

one wavelength (0.5 μm), which is derived from the broad–band measurements. Consequently, the optical depth at 0.5 μm derived from AVHRR differs greatly from that at 0.525 μm observed by SAGE–II in the tropics where dense aerosol clouds existed (Andronova *et al.* 1999). In the present study, a time–dependent, zonally averaged, vertically resolved spectral dataset of the Pinatubo aerosol optical properties covering the time from June 1991 through May 1993 are created for the 24–layer ST–GCM using the method of Stenchikov *et al.* (1998)

2. Surface–Air Temperature Anomalies — Observed Data Analyses

Large surface–air temperature anomalies have been observed after violent volcanic eruptions. The Tambora eruption in 1815, the largest in recent history, caused the "Year without a Summer" (Stothers 1984). Surface–air temperatures were abnormally low in the Northern Hemisphere from late spring to early autumn. Widespread famine killed more than 82,000 people because of crop failures. After the Pinatubo eruption, global–mean surface–air temperature decreased by about 0.5°C in JJA 1992. Smaller cooling occurred in JJA 1993. In DJF 1991–1992 and DJF 1992–1993, relative warmth occurred in the northern–hemisphere high latitudes (Parker *et al.* 1996). However, these observed temperature changes cannot be accounted for solely by the Pinatubo eruption. Events such as El Niños in 1991–1992 and 1993 complicated the interpretation of the causes of the observed temperature changes. Robock and Mao (1995) removed El Niño signals from the observed surface temperature anomalies by formulating a linear regression between the Southern Oscillation Index (SOI) and the high–pass–filtered surface temperature anomalies to quantify the influences of historical volcanic eruptions on surface–air temperature. However, the SOI is not an optimal measure of the patterns of sea–surface temperature (SST) anomalies associated with El Niño events (Barnston 1991). In the present study a more sophisticated statistical tool, the Singular Value Decomposition method (Bretherton *et al.* 1992),

will be used to separate the signals of El Niño events and volcanic eruptions in the observed surface–air temperature changes after the Pinatubo eruption.

3. Numerical Simulations

The complicated interactions among all the processes illustrated in Fig. 1.1 make it impossible to understand their individual impact on climate by performing observational data analyses alone. Numerical models with varying complexity in atmospheric dynamics, aerosol microphysics, radiative transfer and atmospheric chemistry have been used to study the Pinatubo eruption. A few studies have used atmospheric GCMs to simulate the atmospheric temperature and circulation changes. Hansen *et al.* (1992) simulated the surface–air temperature changes using the 9–layer GISS (Goddard Institute for Space Studies) GCM coupled with a non–dynamic mixed–layer ocean model with diffusive heat transport to the deep ocean. Graf *et al.* (1993) investigated the northern–hemisphere circulation and surface–air temperature changes after the Pinatubo eruption by performing perpetual–January simulations using the ECHAM2 GCM. Kinchner and Graf (1995) compared the signals of El Niño and the Pinatubo aerosol forcing in the simulated temperature and circulation in January by also performing perpetual–January simulations using the ECHAM2 GCM. In spite of their success in simulating some of the observed atmospheric temperature and circulation changes, these studies have shortcomings. The GISS 9–layer GCM has a coarse horizontal resolution of 8 by 10 degrees and has only 1–2 layers in the stratosphere. The optical depth of El Chichón was used as a substitute for Mount Pinatubo, with an overall enhancement by a factor of 1.7. Graf *et al.* (1993) and Kinchner and Graf (1995) included the radiative forcing of the Pinatubo aerosol in the ECHAM2 GCM by reducing the downward solar radiative flux at the model top (10 hPa) and by adding anomalous longwave heating rates in the stratosphere computed offline by using another radiation model. Radiative forcing of the Pinatubo eruption was not accurately introduced into these GCMs.

In the present study the dataset of the Pinatubo aerosol optical properties created specifically for the 24–layer ST–GCM based on the method of Stenchikov *et al.* (1998) will be used. Multiple sets of ensemble simulations will be performed by using the 24–layer ST–GCM with prescribed SSTs to study the changes of atmospheric temperature and circulation during the two years following the Pinatubo eruption. Simulated results will be compared to the NCEP/NCAR Reanalysis.

Satellite observations revealed substantial total ozone losses over the globe during a few years following the Pinatubo eruption (Randel *et al.* 1995). Observational data analysis (Angell 1997) indicates that associated with the quasi–biennial oscillation (QBO) of the equatorial zonal wind in the tropical lower stratosphere, there is a quasi–biennial oscillation of temperature. The roles of the observed ozone depletion and the QBO have not been addressed in those earlier GCM simulations. In the present study their roles will be investigated. It should be indicated that recently Kirchner *et al.* (1999) also performed a set of experiments using the ECHAM4 GCM with prescribed SSTs to study the climate responses of the atmosphere to the Pinatubo eruption. They used the dataset of aerosol optical properties created by Stenchikov *et al.* (1998). They also estimated the influences of the ozone depletion and the QBO on the simulated stratospheric temperature.

Among all the previous GCM simulations, only Hansen *et al.* (1996) included the influence of the ocean by coupling the GISS GCM with a non–dynamic mixed–layer ocean model with diffusive heat transport to the deep ocean. It is still not clear how the ocean affected the responses of the atmosphere to the Pinatubo aerosol forcing. In the present study the UIUC 24–layer ST–GCM will be coupled with an 18–layer ocean GCM to estimate the importance of the ocean.

C. Outline of the Present Study

One of the motivations for developing the UIUC 24–layer ST–GCM was to study the Pinatubo eruption. Chapter II introduces the model. Appendix A is dedicated to describing the development and validation of the model in detail. Chapter III describes the reconstruction of the aerosol optical properties of the Pinatubo volcanic aerosol and the calculation of radiative forcing using the UIUC 24–layer ST–GCM. Chapter IV illustrates first the observed changes of atmospheric temperature and circulation following the Pinatubo eruption found in the NCEP/NCAR Reanalysis, and then presents a detailed investigation of the observed surface–air temperature changes. The SVD analysis is used along with other statistical tools to detect and separate the signals of El Niño events and the Pinatubo eruption from the observed surface temperature anomalies over the continents. Chapter V presents the numerical simulations performed and the comparison between simulation and observation. Four ensemble simulations are performed by the 24–layer ST–GCM with prescribed climatological SST or real–time SST, with and without the Pinatubo aerosol. The sensitivity of the simulated temperature anomaly to initial and boundary conditions is examined. The simulated surface and atmospheric temperature anomalies forced by the Pinatubo aerosol forcing are compared to those forced by real–time SST anomalies. The influence of the QBO on the temperature in the tropical lower troposphere is estimated empirically. Two simulations are performed to quantify the influence of ozone depletion on the observed temperature anomalies. Finally, the influence of the ocean on the responses of the atmosphere to the Pinatubo aerosol forcing is investigated by running the coupled 24–layer atmosphere/18–layer ocean GCM. Chapter VI presents the conclusions.